

1 **SARS-CoV-2 S protein ACE2 interaction reveals**  
2 **novel allosteric targets**  
3

4 Palur Raghuvamsi<sup>1†</sup>, Nikhil Tulsian<sup>1,2†</sup>, Firdaus Samsudin<sup>3</sup>, Xinlei Qian<sup>4</sup>,  
5 Kiren Purushotorman<sup>4</sup>, Gu Yue<sup>4</sup>, Mary Kozma<sup>4</sup>, Julien Lescar<sup>5</sup>, Peter  
6 Bond<sup>1,3\*</sup>, Paul MacAry<sup>4\*</sup> and Ganesh Anand<sup>1\*</sup>

7  
8 <sup>1</sup> Department of Biological Sciences, National University of Singapore, 14 Science Drive 4,  
9 Singapore 117543

10 <sup>2</sup> Department of Biochemistry, National University of Singapore, 28 Medical Drive, Singapore  
11 117546

12 <sup>3</sup> Bioinformatics Institute, Agency for Science, Technology, and Research (A\*STAR), 30 Biopolis  
13 Street, Singapore 138671

14 <sup>4</sup> Life Sciences Institute, Centre for Life Sciences, National University of Singapore, 28 Medical  
15 Drive, Singapore 117546

16 <sup>5</sup> School of Biological Sciences, National Technological University, 60 Nanyang Drive, Singapore  
17 637551

18  
19 † These authors contributed equally.

20 \* Correspondence: [dbsgsa@nus.edu.sg](mailto:dbsgsa@nus.edu.sg), [micpam@nus.edu.sg](mailto:micpam@nus.edu.sg), [peterjb@bii.a-star.edu.sg](mailto:peterjb@bii.a-star.edu.sg)

21 **Running Title:** *Spike-ACE2 interactions allosterically prime proteolytic processing of Spike*  
22 *protein*

23 **Keywords:** Spike, ACE2, allostery, proteolysis, virus-host interactions, fusion peptide, SARS-  
24 CoV-2

25 **Abbreviations:** HDXMS, Hydrogen Deuterium Exchange Mass Spectrometry; MD, molecular  
26 dynamics, RFU, Relative Fractional deuterium uptake; RMSF, root mean squared fluctuations;  
27 PCA, Principal Component Analysis; S, Spike; UPLC, Ultra Performance Liquid  
28 Chromatography;

29

30 **Abstract:** The Spike (S) protein is the main handle for SARS-CoV-2 to enter host cells through  
31 surface ACE2 receptors. How ACE2 binding activates proteolysis of S protein is unknown. Here,  
32 we have mapped the S:ACE2 interface and uncovered long-range allosteric propagation of ACE2  
33 binding to sites critical for viral host entry. Unexpectedly, ACE2 binding enhances dynamics at a  
34 distal S1/S2 cleavage site and flanking protease docking site  $\sim 27$  Å away while dampening  
35 dynamics of the stalk hinge (central helix and heptad repeat) regions  $\sim 130$  Å away. This highlights  
36 that the stalk and proteolysis sites of the S protein are dynamic hotspots in the pre-fusion state.  
37 Our findings provide a mechanistic basis for S:ACE2 complex formation, critical for proteolytic  
38 processing and viral-host membrane fusion and highlight protease docking sites flanking the S1/S2  
39 cleavage site, fusion peptide and heptad repeat 1 (HR1) as allosterically exposed cryptic hotspots  
40 for potential therapeutic development.

41

42 **One Sentence Summary:** SARS-CoV-2 spike protein binding to receptor ACE2 allosterically  
43 enhances furin proteolysis at distal S1/S2 cleavage sites

44           The COVID-19 pandemic caused by the SARS-CoV-2 virus has sparked extensive efforts  
45 to map molecular details of its life cycle to drive vaccine and therapeutic discovery.(1) SARS-  
46 CoV-2 belongs to the family of *Coronaviridae* which includes other human pathogens including  
47 common cold causing viruses (hCoV-OC43, HKU and 229E), SARS and MERS-CoV.(2-5)  
48 SARS-CoV-2 has a ~30 Kbp long positive RNA genome with 14 open reading frames, encoding  
49 4 structural proteins: Spike (S) protein, membrane (M) protein, envelope (E) protein and nucleo-  
50 protein; 16 non-structural proteins and 9 accessory proteins.(6-8) An intact SARS-CoV-2 virion  
51 consists of a nucleocapsid core composed of nucleoprotein packaged genomic RNA encapsidated  
52 as a lipid-protein envelope forming a spherical structure of diameter ~100 nm.(9) The viral  
53 envelope is decorated with S, M and E proteins.(9) The S protein is a club-shaped homotrimeric  
54 class I viral fusion protein that has distinctive ‘head’ and ‘stalk’ regions (Fig. 1A).

55           A characteristic feature of SARS-CoV-2 is proteolysis of Pre-fusion S protein by host  
56 proteases into S1 and S2 subunits. The S1 subunit comprises an N-terminal domain (NTD) and a  
57 receptor binding domain (RBD) that interacts with the host receptor Angiotensin converting  
58 enzyme-2 (ACE2)(10, 11) to initiate viral entry into the host.(12) Cryo-electron tomography (cryo-  
59 ET) has been used to capture the distribution and organization of trimeric S protein on the intact  
60 virion,(9) revealing that  $25 \pm 9$  S protein trimers decorate a single virion with a small percentage  
61 (3%) of embedded S proteins in a post-fusion state adopting an extended helical conformation.  
62 The first virus-host interaction is mediated by the viral S protein with the host ACE2 receptor.(10)  
63 Binding to ACE2 primes the S protein for proteolysis at S1/S2 cleavage site into individual S1 and  
64 S2 subunits.(13, 14) The S2 subunit is divided into six constituent domains harboring the  
65 membrane fusion machinery of the virus. These comprise the fusion peptide (FP), heptad repeat  
66 (HR1), heptad repeat 2 (HR2), connector domain (CD), transmembrane domain (TM), and

67 cytoplasmic tail (CT).(15, 16) Extensive structural studies (9, 15, 17, 18) have captured S proteins  
68 of coronaviruses in distinct open- (PDB:6VXX)(15) and closed- (PDB:6VYB)(15) conformational  
69 states with regards the RBD, as well as the ectodomain orientation in the pre- and post-fusion  
70 states, thereby revealing a high intrinsic metastability of the S protein. The S2 subunit promotes  
71 membrane fusion and viral entry (Fig. 1B).

72 Despite extensive cryo-EM studies, how ACE2 binding at the RBD domain primes  
73 enhanced proteolytic processing at the S1/S2 site is entirely unknown. Amide hydrogen/deuterium  
74 exchange mass spectrometry (HDXMS) is a powerful complementary tool for both virus dynamics  
75 (19) and mapping protein-protein interactions.(20) Here, we describe the dynamics of free S  
76 protein, the S:ACE2 complex and describe ACE2 binding-induced allosteric conformational  
77 changes across the distal regions of S protein, particularly at the stalk and protease docking sites  
78 flanking the S1/S2 cleavage sites. These distal ‘hotspots’ are critical for the first step of SARS-  
79 CoV-2 infection and represent novel targets for therapeutic intervention.

## 80 **Results and Discussion**

### 81 **Localizing subunit specific dynamics and domain motions of S protein trimer**

82 Structural snapshots of the ACE2 binding to the SARS-CoV-2 S protein interface have  
83 been obtained with the RBD alone.(10, 16, 21-23) In this study, we have mapped this interface for  
84 the S protein construct (1-1208) with mutations at the S1/S2 cleavage site (PRRAS to PGSAS)  
85 and proline substitution at 986-987,(16) to block proteolysis during expression and purification  
86 (Fig. S1A). The S protein and isolated RBD constructs showed high affinity binding to ACE2 (Fig.  
87 S1B). We measured dynamics of a trimer of this near-full length S protein by amide hydrogen-  
88 deuterium exchange mass spectrometry (HDXMS). Pepsin proteolysis generated 321 peptides  
89 with high signal to noise ratio, accounting for ~87% of the entire S protein (Fig. S2). Glycosylation

90 of at least 22 sites have been predicted on S protein.(24) Average deuterium exchange at these  
91 reporter peptides was monitored for comparative deuterium exchange analysis of S protein, ACE2  
92 receptor and S:ACE2 complex, along with a specific ACE2 complex with the isolated RBD. While  
93 glycosylation is an important posttranslational modification, our HDXMS study has measured  
94 deuterium exchange of non-glycosylated segments of S protein alone. Deuterium exchange ( $t = 1$   
95 and 10 min) across all peptides of the free S protein trimer are shown in (Fig. 2). We built an  
96 integrative model of the full-length S protein trimer using experimental structures of prefusion S  
97 ectodomain in the open conformation (PDB: 6VSB)(16) and the HR2 domain from SARS S  
98 protein as templates. Mapping the relative deuterium exchange across all peptides onto this S  
99 protein model showed the greatest deuterium exchange at the stalk region. (Fig. 2A) This is  
100 consistent with earlier studies showing at least 60° sweeping motions of the three identified hinge  
101 regions of the stalk.(18) This was further verified via all-atom MD simulations of the S protein  
102 model embedded in a viral model membrane, which showed significant motions of the S protein  
103 ectodomain as a result of the flexible stalk region, (Fig. 2B) as well as large atomic fluctuations  
104 around the HR2 domain, compared to the rest of the protein (Fig. S3, Fig. S4).

105 The deuterium exchange heat map showed the highest relative exchange in the S2 subunit  
106 (Fig. S3) and helical segments, while peptides spanning the fusion peptide showed relatively lower  
107 deuterium exchange. Individually, S1 and S2 subunits showed different intrinsic deuterium  
108 exchange kinetics, where the average relative fractional deuterium uptake (RFU) of S1 subunit  
109 (~0.25) was lower than the average RFU (~0.35) of S2 subunit (Fig. S3, Table S1). Moreover,  
110 peptides connecting the RBD to the remainder of the S protein showed greater deuterium  
111 exchange, reflecting its role as a ‘hinge’ facilitating the RBD populating an ensemble of open- and  
112 closed- conformational states (red arrow, Fig. 2C). Indeed, in our simulations of the S protein (Fig.

113 2B), the RBD oriented initially in an ‘up’- conformation exhibited spontaneous motion towards  
114 the ‘down’- conformation relative to the hinge region (Fig. 2D, Fig. S4A). Interestingly, a part of  
115 the receptor binding motif, specifically residues 476-486, exhibited a higher degree of flexibility  
116 based on its average atomic fluctuations (Fig. 2A, 4C), suggesting that binding to ACE2 receptor  
117 would be required to stabilize its motion.

118 The NTD of the S protein showed low overall RFU (~0.2), consistent with its well-  
119 structured arrangement of  $\beta$ -sheets connected by loops (Fig. 1B). Importantly, certain regions  
120 showed significantly higher deuterium exchange (~0.4), of which two loci (136-143, 243-265)  
121 span the dynamic interdomain interactions with the RBD. This is supported by the high per-residue  
122 root mean square fluctuations (RMSF) and large principal motions observed for residues 249-259  
123 during simulations (Fig. 2C, Fig. S4C). One locus (291-303) at the C-terminal end of the NTD  
124 connecting to the RBD showed high deuterium exchange, indicative of relative motions of the two  
125 domains. The RBD (Fig. 1D) showed relatively higher deuterium exchange (RFU ~0.35), with the  
126 peptides spanning the hinge-regions (318-336) showing greatest deuterium exchange (~0.6).  
127 Peptides spanning residues 351-375 and 432-452 showed significantly increased deuterium  
128 uptake, and these correspond to the NTD interdomain interaction sites. Interestingly, loci of the  
129 RBD implicated in the interface (453-467, 491-510) with ACE2 showed relative higher exchange.

130 Overall, the S2 subunit showed relatively higher RFU than the S1 subunit, with each  
131 domain exhibiting specific conformational changes (Fig. 1E, Fig. S4). Peptides spanning the  
132 region immediately downstream of the S1/S2 cleavage site showed the highest deuterium uptake  
133 (0.6), reflecting the rapid dynamics it undergoes for facilitating cleavage of S protein into two  
134 subunits. Congruently, our MD simulations revealed the unstructured loop housing the S1/S2  
135 cleavage site (residues 677-689) to be highly dynamic (Figure S4C), with RMSFs reaching >1.0

136 nm. It is important to note that the S1/S2 cleavage site has been abrogated in the construct of the  
137 S protein used in this study to block proteolytic processing into S1 and S2 subunits during  
138 expression in host cells. We thus observed lower deuterium uptake (and lower RMSF values) at  
139 peptides in the central helix and connector domain, suggesting that these act as the central core of  
140 prefusion S, while the peptides spanning hinge-segments and heptad repeats (HR1 and HR2)  
141 showed high deuterium uptake and RMSF values, indicative of the inherent metastability of S to  
142 adopt prefusion, fusion and post-fusion conformations.

### 143 **Domain-specific and global effects of ACE2 binding to the RBD**

144 Comparative HDXMS analysis of the S protein and S:ACE2 complex revealed large-scale  
145 effects upon binding of ACE2. The main target for direct interactions was the RBD. We therefore  
146 set out to characterize the effects of ACE2 binding with RBD ('RBD<sub>S</sub>') present on full S protein  
147 (Fig. 4A, 4B) and compared this to an isolated construct of the RBD ('RBD<sub>isolated</sub>') (Fig. 3, Fig.  
148 S6). Several peptides of the RBD<sub>S</sub> showed decreased exchange upon complexation with ACE2  
149 (Fig. 3B). These include peptides 340-359, 400-420, 432-452 and 487-502 in the RBD<sub>S</sub>:ACE2  
150 complex (Fig. 4). These sites are consistent with the interface of the SARS-CoV-2 S protein RBD  
151 bound to the ACE2 receptor resolved by X-ray crystallography.<sup>(10)</sup> The high-resolution structures  
152 showed that the RBD and ACE2 receptor interact via an extensive interface. However, not all  
153 peptides at the interface contribute equally to the binding energetics. HDXMS reveals the residues  
154 at the core of this interface to be those within peptides spanning residues 340-359, 400-420, 432-  
155 452 and 491-510 (Fig. 4A, 4D, Fig. S3). Interestingly, loci showing large-magnitude deuterium  
156 exchange correlate to mutational hotspots<sup>(25)</sup>.

157 A close-up of RBD<sub>isolated</sub>:ACE2 complex also showed decreased exchange in peptides  
158 spanning these regions (Fig. 3). However, the magnitude of decrease in exchange was significantly

159 greater in RBD<sub>isolated</sub> than in RBD<sub>S</sub>, indicating the higher flexibility in the full-length S trimer than  
160 in free RBD. High resolution structures have identified the RBD interface interacting with ACE2  
161 spanning the peptide covering residues 448-501 (Y449, Y453, N487, Y489, G496, T500, G502,  
162 Y505, L455, F456, F486, Q493, Q498 and N501) using only the RBD from the S protein.(23)  
163 Cryo-EM studies have shown that each RBD in the trimeric S protein can adopt an open  
164 conformation irrespective of other RBDs, indicating an absence of cooperativity between the three  
165 RBDs within a trimer.(9) Therefore, we compared the deuterium exchange profiles of RBD<sub>isolated</sub>  
166 with RBD<sub>S</sub> and observed differences in dynamics imposed by quaternary contacts (Fig. 3A, Fig.  
167 3B). Overall, the loci with high and low deuterium exchange profiles were similar when compared  
168 between RBD<sub>isolated</sub> and RBD<sub>S</sub>, both at the disordered ACE2 receptor binding region as well as the  
169 folded region at the N- and C -termini. In solution RBD<sub>S</sub> toggles between open- and closed-  
170 conformations resulting in an average readout of deuterium exchange measurements.

171 ACE2 binding to RBD<sub>isolated</sub> and RBD<sub>S</sub> resulted in similar effects, where we observed  
172 deuterium exchange protection at the peptide regions spanning the known binding interface of  
173 RBD. Notably, increased deuterium exchange was observed at the hinge region (Fig. 3C, Fig. S4)  
174 indicating allosteric conformational changes, associated with restricting the open- and closed-  
175 states interconversion. Therefore, the destabilization/ local unfolding observed at the hinge region  
176 as a result of ACE2 binding enables RBD to maintain open conformation. It therefore seems likely  
177 that small molecules and biologics targeting the hinge region to lock RBD in the closed state would  
178 be of potential high therapeutic value.

179 **ACE2 binding at the RBD is allosterically propagated to the S1/S2 cleavage site and Heptad**  
180 **Repeat**



181 Unexpectedly, ACE2 binding at the RBD induced large-scale changes in deuterium  
182 exchange in distal regions of the S protein. Some of the peptides in the stalk of S protein showed  
183 decreased exchange in the S:ACE2 complex (Fig. 4C, 4D). This indicates that ACE2 receptor  
184 interactions stabilized the hinge dynamics. Decreased exchange was also seen in the distal sites in  
185 the S2 subunit, localized at the fusion peptide locus and central helix (CH). Interestingly, increased  
186 exchange was seen in multiple peptides flanking the S1/S2 cleavage site, HR1 domain and  
187 critically at the S1/S2 cleavage sites (Fig. 4D). Even though the construct used in this study has  
188 the proteolysis site mutated, it still resulted in increased dynamics at this S1/S2 locus. Furthermore,  
189 this region exhibited high RMSF values during simulations. (Fig. S4B). These results clearly  
190 indicate that ACE2 binding induces allosteric enhancement of dynamics at this locus, providing  
191 mechanistic insights into the conformational switch from the pre-fusion to fusogenic intermediate.  
192 Differences in deuterium exchange between free S protein and S:ACE2 complex shows  
193 stabilization at ACE2 interacting site and local destabilization at peptides juxtaposed to S1/S2  
194 cleavage site (residues 931-938). This suggests that ACE2 binding potentiates peptide of residues  
195 931-938 and other high exchanging regions flanking the S1/S2 cleavage site for enhanced furin  
196 protease binding and cleavage. Importantly, these results suggest that the S1/S2 cleavage site is a  
197 critical hotspot for S protein dynamic transitions for viral entry into the host, and therefore  
198 represents a new target for inhibitory therapeutics against the virus.

### 199 **Dynamics of ACE2 with RBD and S protein provides insights into viral-entry into host**

200 Considering the indispensable role of ACE2 binding in SARS-CoV-2 infection, it is crucial to  
201 assess the effects of S protein and RBD binding on ACE2 dynamics. We therefore mapped the  
202 corresponding binding sites of RBD, both isolated and within the Spike, on ACE2. The S:ACE2  
203 complex represents the prefusion pre-cleavage state wherein full-length S protein is bound to the

204 ACE2 receptor (Fig. 1B ii), while the RBD<sub>isolated</sub>:ACE2 complex represents the post-furin cleavage  
205 product formed by the S1 subunit and ACE2 (Fig. 1B iii). Previous studies have shown that 14 key  
206 amino acids of RBD interact with ACE2, wherein mutations at 6 amino acids resulted in higher  
207 binding affinity of SARS-CoV-2.(26) SARS-CoV-2 adopted a different binding mode to ACE2 as  
208 a superior strategy for infection in comparison to SARS-CoV-1. A crystal structure of  
209 RBD<sub>isolated</sub>:ACE2 complex has identified 24 key ACE2 residues, spanning across peptides 16-45,  
210 79-83, 325-330, 350-357 and Arg393.(27) While most of these residues are conserved in binding  
211 to both SARS-CoV-1 and SARS-CoV-2, Arg393 and residues 325-330 are unique to SARS-CoV-  
212 1 interaction.(25) Interestingly, we observed increased deuterium exchange at these residues in the  
213 S:ACE2 complex compared to ACE2 alone (Fig. S8). Identifying the intrinsic dynamics and  
214 allosteric changes due to binding could potentially better inform drug development.

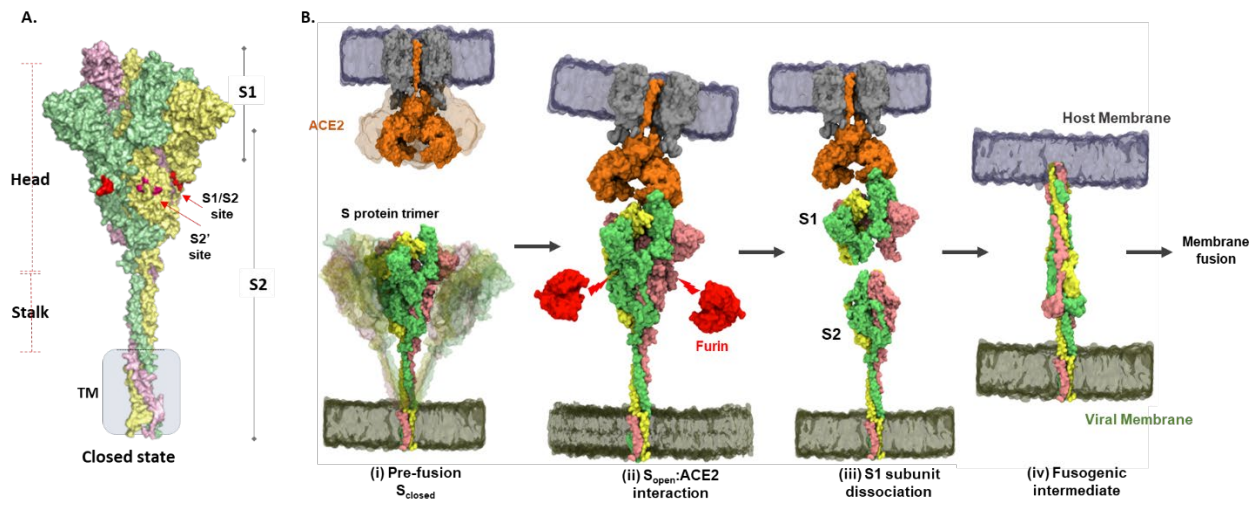
215 Simulations of the ACE2 dimer complexed with the B<sup>0</sup>AT1 amino acid transporter (PDB:  
216 6M1D)(12) in a model epithelial membrane revealed a large motion of the peptidase domain (PD),  
217 which recognizes the S protein RBD, with respect to the transmembrane and juxtamembrane  
218 domains (Fig. S7). This large motion is reminiscent of the flexible tilting displayed by the S protein  
219 ectodomain itself, suggesting that both S protein and ACE2 have adaptable hinges that allow for  
220 orientational freedom of the domains involved in recognition. To understand how S protein  
221 binding affects ACE2 dynamics, we performed HDXMS experiments of monomeric ACE2 alone,  
222 S:ACE2 and RBD:ACE2 complexes (Fig. S7, Fig. S8) and mapped the deuterium exchange values  
223 on a deletion construct of ACE2 (PDB: 1R42)(27) (Fig. S7, Fig. S8). We observed a reduction in  
224 deuterium exchange across both RBD<sub>isolate</sub>:ACE2 and larger S:ACE2 complexes compared to free  
225 ACE2 (Figure S8B and S8C). Differences in deuterium exchange between RBD<sub>isolated</sub>:ACE2  
226 complex and free ACE2 showed that RBD binding stabilizes ACE2 globally, specifically large

227 differences at the binding site (peptides 21-29, 30-39, and 75-92), and also at distal regions  
228 (peptides 121-146, 278-292, 575-586) from RBD binding site of ACE2 (Fig. S8D). Cryo-EM  
229 studies have shown that a dimeric full length ACE2 receptor can stably bind to one trimer of the S  
230 protein.(12)

### 231 **Conclusions**

232 Here a combination of HDXMS and MD simulations provide a close-up of S protein  
233 dynamics in the pre-fusion, ACE2 bound and other associated conformations. Our results reveal  
234 the energetics of the S:ACE2 complex interface. ACE2 binding to the isolated RBD and S protein  
235 alike lead to binding and stabilization. Interestingly, ACE2 binding to the RBD induces global  
236 conformational changes across the entire S protein. Importantly, the stalk region undergoes  
237 dampening of conformational motions while causing increased deuterium exchange in the protease  
238 sites. Regions highlighting the allosteric propagation of ACE2 binding represent cryptic targets  
239 for small molecule inhibitor/antibody development as therapeutics.

324 **Figures**

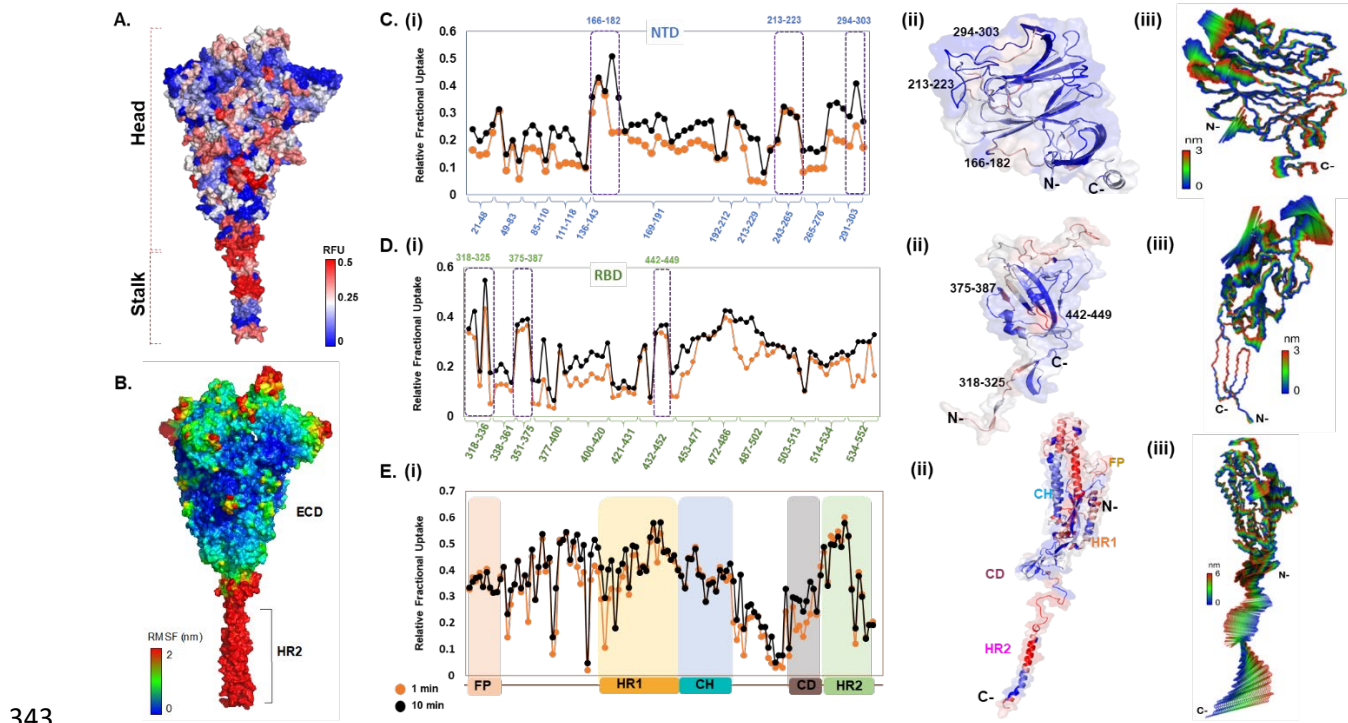


325

326 **Figure 1: Structure and domain organization of trimeric S protein showing steps in the virus-**  
327 **host entry initiated by S recognition and binding to ACE2 receptor**

328 **A.** Prefusion S protein trimer in closed conformational state, with monomers shown in yellow,  
329 green and pink. S protein construct (1-1245) used in this study showing head, stalk and  
330 transmembrane (TM) segments as generated by integrative modeling. The S1/S2 and S2' cleavage  
331 sites are in red. Proteolytic processing (Furin) of S protein generates S1 and S2 subunits. **B.**  
332 Schematic of viral entry into host cell mediated by S:ACE2 interactions as previously outlined(28):  
333 (i) Intrinsic dynamics of pre-fusion S protein trimer decorating SARS-CoV-2 and host ACE2  
334 dimeric structure showing sweeping motions of S protein and ACE2 to facilitate S:ACE2  
335 recognition. (ii) In the open conformation ( $S_{open}$ ), RBD adopts an 'up' orientation to recognize and  
336 bind the host membrane-bound ACE2 receptor (PDB: 1R42). ACE2 binding induces  
337 conformational changes promoting Furin (red) proteolysis at the S1/S2 cleavage site (red arrows,  
338 leading to dissociation of S1 and S2 subunits, mechanism of which is unknown. (iii) The residual  
339 ACE2-bound S1 subunit stably bound to ACE2 and S2 subunits dissociate (iv) Conformational

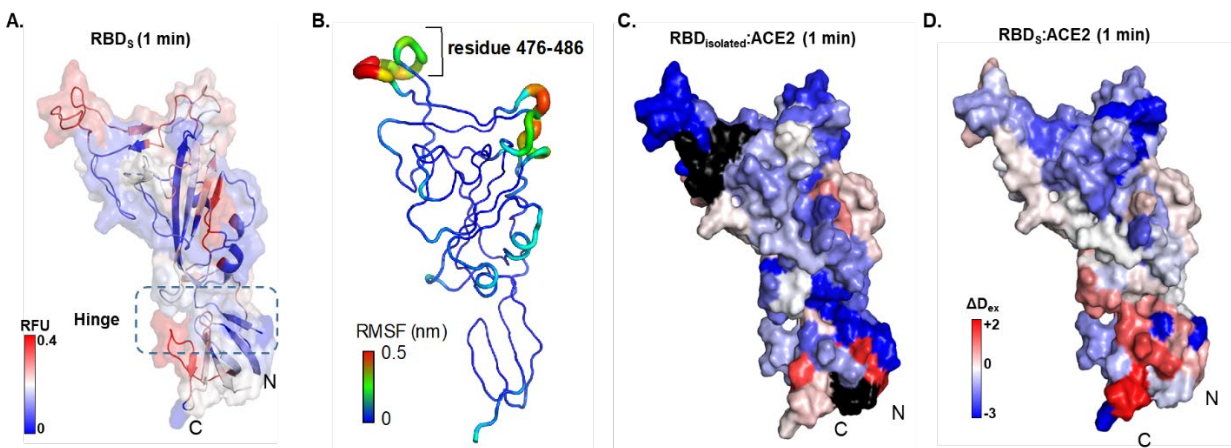
340 changes in the separated S2 subunit promote formation of an extended helical fusogenic  
 341 intermediate (PDB ID: 6M3W),(17) for fusion into the host cell membrane, membrane fusion and  
 342 viral entry into the host cell.(11)



344 **Figure 2: Deuterium exchange heat map and MD simulations reveal domain-specific**  
 345 **conformational dynamics of pre-fusion S protein trimer.**

346 **A.** Deuterium exchange heat map (shades of blue (low exchange) and red (high exchange)) of S  
 347 protein (residues 1-1208) at t = 1 min deuterium exchange mapped onto structure of S protein. **B.**  
 348 Per-residue root mean square fluctuations (RMSF) of the S protein (without TM domain) mapped  
 349 on to the surface of the S trimer. Deuterium exchange based dynamics across N-terminal domain  
 350 **(C)**, RBD **(D)**, and the S2 subunit **(E)**. (i) Relative fractional deuterium uptake (RFU) plots of  
 351 NTD, RBD and the S2 subunit at 1 min (orange) and 10 min (black) deuterium exchange times is  
 352 shown, with pepsin digest fragments displayed from N to C-terminus (X-axis), (see Fig. S2, Table

353 S1). (ii) Close-up of the structures of NTD (21-303), RBD (318-552) and the S2 subunit (810-  
354 1208). Peptides spanning NTD-RBD interaction sites (166-182, 213-223, 294-303, 318-325, 375-  
355 387 and 442-449) showing relatively high deuterium exchange at  $t=1$  min are highlighted. (iii)  
356 The first principal motion and RMSF values of backbone atoms on the NTD, RBD and the S2  
357 subunits. Residues with high RMSF are labelled. Different domains (FP, HR1, CH, CD, HR2)  
358 showing domain-specific RFU changes are labeled.  
359

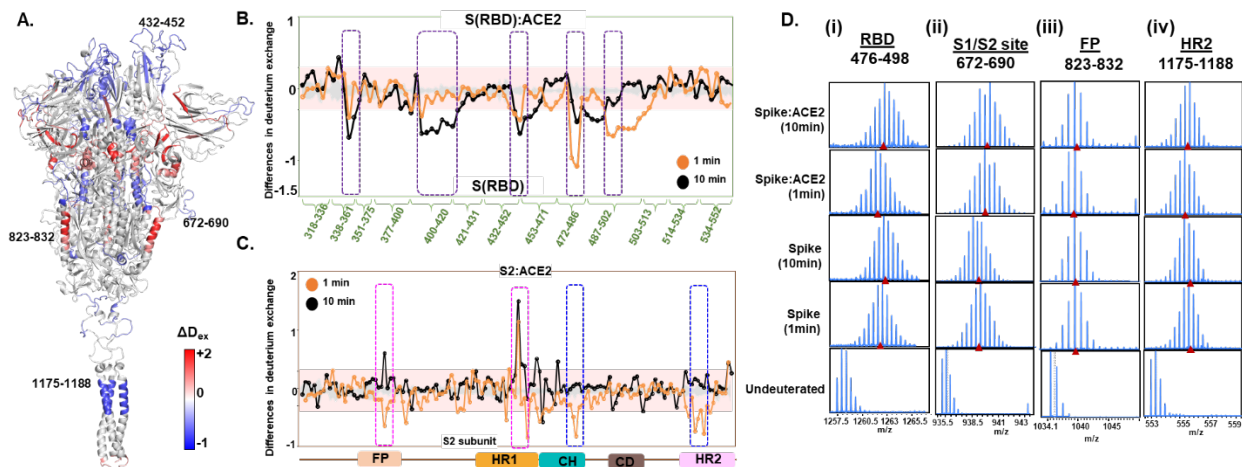


360

### 361 **Figure 3. Map of RBD<sub>isolated</sub>:ACE2 interactions**

362 (A) Relative fractional deuterium uptake values at  $t = 1$  min for RBD (314-547) of S protein  
363 (RBD<sub>s</sub>) mapped on to the structure of RBD extracted from S protein model (see Table S2). High  
364 and low exchanging regions are represented as shown in key, and regions with no coverage are  
365 shown in black. (B) The RMSF values of backbone atoms on the RBD showing residues with high  
366 RMSF (476-486), as per key. Differences in deuterium exchanged between RBD<sub>isolated</sub>:ACE2  
367 complex and free RBD<sub>isolated</sub> (C) and RBD<sub>spike</sub>:ACE with free RBD<sub>spike</sub> (D) at 1min of deuterium  
368 labelling are mapped on to the structure of RBD. Protection from deuterium uptake and increases  
369 in exchange are indicated in blue and red respectively. Regions with no coverage are in black.





370

### 371 **Figure 4: ACE2 interaction induce large scale allosteric changes across S protein**

372 **(A)** Differences in deuterium exchange ( $\Delta D_{ex}$ ) ( $t = 1$  min) in S protein upon binding ACE2 showing  
 373 decreased (blue) and increased (red) deuterium exchange, mapped onto structure of S protein.  
 374 These differences in deuterium exchange for peptides from **(B)** RBD and S2 subunit **(C)** for pepsin  
 375 digest fragments (X-axis) are shown. Difference cutoff  $\pm 0.3$  D is the deuterium exchange  
 376 significance threshold indicated by pink shaded box with standard error values in gray. Positive  
 377 differences ( $>0.3$  D) denote increased deuterium exchange and negative differences ( $<-0.3$  D)  
 378 denote decreased deuterium exchange in S protein bound to ACE2. **(B)** Peptides spanning residues  
 379 interacting with ACE2 are in purple. **(C)** Peptides spanning fusion peptide (FP) and HR1 are  
 380 highlighted in pink boxes, while peptides spanning central helix (CH) and heptad repeat 2 (HR2)  
 381 are in blue. **D.** Stacked mass spectra with isotopic envelopes after deuterium exchange ( $t = 1, 10$   
 382 min) for select peptides from (i) RBD (residues 476-498), (ii) S1/S2 cleavage site (residues 672-  
 383 690), (iii) fusion peptide (residues 823-832) and (iv) HR2 (residues 1175-1188) are shown for the  
 384 S protein and S:ACE2 complex. Mass spectra of the equivalent undeuterated peptide are shown  
 385 for reference. The centroid masses are indicated by red arrow-heads.

## 240 References

- 241 1. N. Bar-Zeev, T. Inglesby, COVID-19 vaccines: early success and remaining challenges. *The Lancet*.  
242 2. V. M. Corman, D. Muth, D. Niemeyer, C. Drosten, Hosts and Sources of Endemic Human  
243 Coronaviruses. *Adv Virus Res* **100**, 163-188 (2018).  
244 3. J. R. St-Jean *et al.*, Human respiratory coronavirus OC43: genetic stability and neuroinvasion. *J*  
245 *Virology* **78**, 8824-8834 (2004).  
246 4. S. K. P. Lau *et al.*, Coronavirus HKU1 and other coronavirus infections in Hong Kong. *J Clin Microbiol*  
247 **44**, 2063-2071 (2006).  
248 5. S. L. Warnes, Z. R. Little, C. W. Keevil, Human Coronavirus 229E Remains Infectious on Common  
249 Touch Surface Materials. *mBio* **6**, e01697-01615 (2015).  
250 6. S. Su *et al.*, Epidemiology, Genetic Recombination, and Pathogenesis of Coronaviruses. *Trends*  
251 *Microbiol* **24**, 490-502 (2016).  
252 7. K. G. Andersen, A. Rambaut, W. I. Lipkin, E. C. Holmes, R. F. Garry, The proximal origin of SARS-  
253 CoV-2. *Nat Med* **26**, 450-452 (2020).  
254 8. Y. J. Tan, S. G. Lim, W. Hong, Characterization of viral proteins encoded by the SARS-coronavirus  
255 genome. *Antiviral Res* **65**, 69-78 (2005).  
256 9. Z. Ke *et al.*, Structures and distributions of SARS-CoV-2 spike proteins on intact virions. *Nature*,  
257 (2020).  
258 10. J. Lan *et al.*, Structure of the SARS-CoV-2 spike receptor-binding domain bound to the ACE2  
259 receptor. *Nature* **581**, 215-220 (2020).  
260 11. M. Hoffmann *et al.*, SARS-CoV-2 Cell Entry Depends on ACE2 and TMPRSS2 and Is Blocked by a  
261 Clinically Proven Protease Inhibitor. *Cell* **181**, 271-280.e278 (2020).  
262 12. R. Yan *et al.*, Structural basis for the recognition of SARS-CoV-2 by full-length human ACE2. *Science*  
263 **367**, 1444-1448 (2020).  
264 13. A. C. Walls *et al.*, Tectonic conformational changes of a coronavirus spike glycoprotein promote  
265 membrane fusion. *Proceedings of the National Academy of Sciences*, 201708727 (2017).  
266 14. N. Vankadari, Structure of Furin Protease Binding to SARS-CoV-2 Spike Glycoprotein and  
267 Implications for Potential Targets and Virulence. *The Journal of Physical Chemistry Letters* **11**,  
268 6655-6663 (2020).  
269 15. A. C. Walls *et al.*, Structure, Function, and Antigenicity of the SARS-CoV-2 Spike Glycoprotein. *Cell*  
270 **181**, 281-292.e286 (2020).  
271 16. D. Wrapp *et al.*, Cryo-EM structure of the 2019-nCoV spike in the prefusion conformation. *Science*  
272 **367**, 1260-1263 (2020).  
273 17. X. Fan, D. Cao, L. Kong, X. Zhang, Cryo-EM analysis of the post-fusion structure of the SARS-CoV  
274 spike glycoprotein. *Nat Commun* **11**, 3618 (2020).  
275 18. B. Turonova *et al.*, In situ structural analysis of SARS-CoV-2 spike reveals flexibility mediated by  
276 three hinges. *Science*, (2020).  
277 19. X. X. Lim *et al.*, Conformational changes in intact dengue virus reveal serotype-specific expansion.  
278 *Nat Commun* **8**, 14339 (2017).  
279 20. X. X. Lim *et al.*, Epitope and Paratope Mapping Reveals Temperature-Dependent Alterations in  
280 the Dengue-Antibody Interface. *Structure* **25**, 1391-1402.e1393 (2017).  
281 21. A. Ali, R. Vijayan, Dynamics of the ACE2-SARS-CoV-2/SARS-CoV spike protein interface reveal  
282 unique mechanisms. *Scientific Reports* **10**, 14214 (2020).  
283 22. K. K. Chan *et al.*, Engineering human ACE2 to optimize binding to the spike protein of SARS  
284 coronavirus 2. *Science* **369**, 1261-1265 (2020).



- 285 23. Q. Wang *et al.*, Structural and Functional Basis of SARS-CoV-2 Entry by Using Human ACE2. *Cell*  
286 **181**, 894-904.e899 (2020).  
287 24. Y. Watanabe, J. D. Allen, D. Wrapp, J. S. McLellan, M. Crispin, Site-specific glycan analysis of the  
288 SARS-CoV-2 spike. *Science* **369**, 330-333 (2020).  
289 25. Y. Wang, M. Liu, J. Gao, Enhanced receptor binding of SARS-CoV-2 through networks of hydrogen-  
290 bonding and hydrophobic interactions. *Proceedings of the National Academy of Sciences* **117**,  
291 13967-13974 (2020).  
292 26. F. Li, W. Li, M. Farzan, S. C. Harrison, Structure of SARS coronavirus spike receptor-binding domain  
293 complexed with receptor. *Science* **309**, 1864-1868 (2005).  
294 27. P. Towler *et al.*, ACE2 X-ray structures reveal a large hinge-bending motion important for inhibitor  
295 binding and catalysis. *J Biol Chem* **279**, 17996-18007 (2004).  
296 28. J. Shang *et al.*, Structure of mouse coronavirus spike protein complexed with receptor reveals  
297 mechanism for viral entry. *PLOS Pathogens* **16**, e1008392 (2020).

298

299 **Acknowledgements:** We thank Dr. Lu Gan, Dept. of Biological Sciences, National University of  
300 Singapore for helpful discussions. We thank Protein Production Platform of Nanyang  
301 Technological University for their help in making the RBD and ACE2 expression constructs and  
302 small-scale protein expression tests. HDXMS experiments were carried out as a fee for service at  
303 the Singapore National Laboratory for Mass Spectrometry (SingMass) funded by NRF, Singapore.  
304 P.V.R. was supported by research scholarship from National University of Singapore, Singapore.  
305 N.K.T. was supported by research grant from Ministry of Education, Singapore awarded to G.S.A.  
306 (MOE2017-T2-A40-112). This work was supported by BII of A\*STAR. Simulations were  
307 performed on the petascale computer cluster ASPIRE-1 at the National Supercomputing Centre of  
308 Singapore (NSCC) and the A\*STAR Computational Resource Centre (A\*CRC). **Author**  
309 **Contributions:** Conceptualization – P.V.R., N.K.T., P.A.M., G.S.A., P.J.B.; Funding acquisition  
310 – P.A.M.; Investigation – P.V.R., N.K.T., F.S., X.Q., K.P., G.Y., M.M.K.; Methodology – P.V.R.,  
311 N.K.T., F.S.; Resources – P.V.R., N.K.T., P.A.M., G.S.A., P.J.B.; Supervision & Validation;  
312 Visualization – P.V.R., N.K.T., F.S.; Writing - original draft – P.V.R., N.K.T., G.S.A., F.S., P.J.B.;  
313 Writing – review & editing - P.V.R., N.K.T., G.S.A., F.S., P.J.B., P.A.M. **Competing interests:**  
314 Authors declare no competing interests. **Data and Materials Availability:** All data is available in  
315 the main text or the supplementary materials. Data, code and materials provided upon request.

316

## 317 **SUPPLEMENTARY MATERIALS**

318 Materials and Methods

319 Figs. S1 to S8

320 Tables S1 to S3

321 References (29-55)

322

323

1  
2  
3  
4  
5  
6  
7  
8  
9  
10  
11  
12  
13  
14  
15  
16  
17  
18  
19  
20  
21  
22  
23  
24  
25  
26  
27  
28  
29  
30

# Supplementary Materials for **SARS-CoV-2 S protein ACE2 interaction reveals novel allosteric targets**

Palur Raghuvamsi<sup>1†</sup>, Nikhil Tulsian<sup>1,2†</sup>, Firdaus Samsudin<sup>3</sup>, Xinlei Qian<sup>4</sup>,  
Kiren Purushotorman<sup>4</sup>, Gu Yue<sup>4</sup>, Mary Kozma<sup>4</sup>, Julien Lescar<sup>5</sup>, Peter  
Bond<sup>1,3\*</sup>, Paul MacAry<sup>4\*</sup> and Ganesh Anand<sup>1\*</sup>

<sup>1</sup> Department of Biological Sciences, National University of Singapore, 14 Science Drive 4,  
Singapore 117543

<sup>2</sup> Department of Biochemistry, National University of Singapore, 28 Medical Drive, Singapore  
117546

<sup>3</sup> Bioinformatics Institute, Agency for Science, Technology, and Research (A\*STAR), 30 Biopolis  
Street, Singapore 138671

<sup>4</sup> Life Sciences Institute, Centre for Life Sciences, National University of Singapore, 28 Medical  
Drive, Singapore 117546

<sup>5</sup> School of Biological Sciences, National Technological University, 60 Nanyang Drive, Singapore  
637551

† These authors contributed equally.

\* Correspondence: [dbsgsa@nus.edu.sg](mailto:dbsgsa@nus.edu.sg), [micpam@nus.edu.sg](mailto:micpam@nus.edu.sg), [peterjb@bii.a-star.edu.sg](mailto:peterjb@bii.a-star.edu.sg)

## **This PDF file includes:**

Materials and Methods  
References (29-55)  
Figs. S1 to S8

## **Other Supplementary Materials for this manuscript include the following:**

Captions for Data S1 to S3

## 31 **Materials and Methods**

### 32 Materials

33 Mass Spectrometry grade acetonitrile, formic acid and water were from Fisher Scientific  
34 (Waltham, MA); Deuterium oxide was from Cambridge Isotope Laboratories (Tewksbury, MA).  
35 All reagents and chemicals were research grade or higher and obtained from Merck-Sigma-Aldrich  
36 (St. Louis, MO).

37

### 38 Methods

39

#### 40 **Transient expression and purification of recombinant SARS-CoV2 Spike, RBD and ACE2** 41 **receptor**

42 A near full-length Spike (S) protein, excluding transmembrane domain and cytoplasmic  
43 tail, of SARS-CoV-2 (1-1208; Wuhan-Hu-1; GenBank: QHD43416.1) was codon optimized for  
44 mammalian cell expression and cloned into pTT5 expression vector (National Research Council  
45 Canada, NRCC) with a twin strep tag at the C-terminus (Twist Biosciences). This double mutant  
46 Spike construct was generated by mutating RRAR (682-685) into GSAS and residues KV (986-  
47 987) into PP. A gene encoding SARS-CoV-2-RBD (319-591 of SARS-CoV-2 Spike) (BioBasic)  
48 was cloned into the expression vector pHLmMBP-10 (Addgene) following the N-terminal His and  
49 mMBP tag. A gene encoding human ACE2 (residues 21-597; GenBank: AB046569.1) fused to a  
50 C-terminal Fc tag (Biobasic) was cloned into vector pHL-sec (Addgene) between the signal  
51 peptide and c-terminal His tag. SARS-CoV-2- Spike constructs were expressed in HEK293-6E  
52 (NRCC) using polyethylenimine (PEI) as the transfection reagent while the isolated RBD  
53 ('RBD<sub>isolated</sub>') and ACE2 constructs were expressed in Expi293F using the Expi293 System  
54 (Thermo Fisher). Culture supernatant was harvested on day 7 for HEK293-6E expression and day  
55 5 for Expi293F expression. Spike proteins were affinity purified using Strep-Tactin®XT column  
56 (IBA). RBD protein was affinity purified using cOmplete™ His-Tag Purification column (Merck).  
57 ACE2 receptor was affinity purified using HiTrap® MabSelect™ SuRe™ column (GE  
58 Healthcare). Purified proteins were concentrated and buffer exchanged into PBS using VivaSpin  
59 (Sartorius) and the purity was assessed by denaturing polyacrylamide gel electrophoresis (Fig.  
60 S1A).

#### 61 **Deuterium labelling and quench conditions**

62 Recombinant purified S protein (8  $\mu$ M), ACE2 receptor (52  $\mu$ M) and RBD (67  $\mu$ M)  
63 solubilized in phosphate buffer (PBS, pH 7.4) were incubated at 37°C in PBS buffer reconstituted  
64 in D<sub>2</sub>O (99.90%) resulting in a final D<sub>2</sub>O concentration of 90%. S:ACE2 and RBD:ACE2  
65 complexes (K<sub>D</sub> of ~15 nM and ~150 nM, respectively)(29) were pre-incubated at 37°C for 30 min  
66 in a molar ratio of 1:1 to achieve >90% binding prior to each hydrogen-deuterium exchange  
67 reaction. Deuterium labeling was performed for 1 min, 10 min and 100 min for isolated construct  
68 of RBD, free ACE2, and RBD<sub>isolated</sub>:ACE2 complex. For isolated S protein and S:ACE2 complex

69 1 min and 10 min labelling timescales were used. Pre-chilled quench solution 1.5 M GnHCl and  
70 0.25 M Tris(2-carboxyethyl) phosphine-hydrochloride (TCEP-HCl) was added to deuterium  
71 exchange reaction mixture to lower the  $\text{pH}_{\text{read}}$  to  $\sim 2.5$  and lower temperature to  $\sim 4^\circ\text{C}$ . Next, the  
72 quenched reaction was incubated at  $4^\circ\text{C}$  on ice for 1 min followed by pepsin digestion.

### 73 **Mass Spectrometry and peptide identification**

74  $\sim 100$  pmol quenched samples were injected onto chilled nanoUPLC HDX sample manager  
75 (Waters, Milford, MA). The injected samples were subjected to online digestion using  
76 immobilized Waters Enzymate BEH pepsin column ( $2.1 \times 30$  mm) in 0.1% formic acid in water  
77 at  $100 \mu\text{l}/\text{min}$ . Simultaneously, the proteolyzed peptides were trapped in a  $2.1 \times 5$  mm C18 trap  
78 (ACQUITY BEH C18 VanGuard Pre-column,  $1.7 \mu\text{m}$ , Waters, Milford, MA). Following pepsin  
79 digestion, the proteolyzed peptides were eluted using acetonitrile gradient of 8 to 40 % in 0.1 %  
80 formic acid at a flow rate of  $40 \mu\text{l min}^{-1}$  into reverse phase column (ACQUITY UPLC BEH C18  
81 Column,  $1.0 \times 100$  mm,  $1.7 \mu\text{m}$ , Waters) pumped by nanoACQUITY Binary Solvent Manager  
82 (Waters, Milford, MA). Electrospray ionization mode was used to ionize peptides sprayed onto  
83 SYNAPT G2-Si mass spectrometer (Waters, Milford, MA) acquired in  $\text{HDMS}^{\text{E}}$  mode of detection  
84 and measurement. A flow rate of  $5 \mu\text{l}/\text{min}$  was used to inject  $200 \text{ fmol } \mu\text{l}^{-1}$  of  $[\text{Glu}^1]$ -fibrinopeptide  
85 B ( $[\text{Glu}^1]$ -Fib) into mass spectrometer for lockspray correction.

86 Undeuterated protein samples were used to identify sequences from mass spectra data (in  
87  $\text{HDMS}^{\text{E}}$  mode) using Protein Lynx Global Server (PLGS) v3.0. Peptide identification search was  
88 performed against a separate sequence database of each protein sequence along with its respective  
89 affinity purification tag sequences. In the PLGS search parameters, i) no specific protease and ii)  
90 no variable N-linked glycosylation modification options were selected for sequence identification.  
91 The identified peptides were further filtered using a minimum intensity cutoff of 2500 for product  
92 and precursor ions, minimum products per amino acids of 0.2 and a precursor ion mass tolerance  
93 of  $<10$  ppm using DynamX v.3.0 (Waters, Milford, MA) and tested for pepsin cleavage  
94 specificity.<sup>(30)</sup> Peptides independently identified under the specified condition and present in at  
95 least in two out of three undeuterated samples were retained for HDXMS analysis. S protein  
96 contains 22 variable glycosylation sites<sup>(31)</sup> out of which we identified peptides spanning 12  
97 glycosylation sites in our sample (Fig. S2). For ACE2, we obtained 4 peptides overlapping the  
98 glycosylation sites (Fig S7). Relative fractional deuterium uptake (RFU) is the ratio of number of  
99 deuterons exchanged to the total number of exchangeable amides of the peptide. Centroid masses  
100 of undeuterated reference spectra were subtracted from equivalent spectra of peptides showing  
101 deuterium exchange to calculate the average deuterons exchanged with time for each peptide.  
102 Deuterium exchange plots, relative deuterium exchange and difference plots were obtained from  
103 DynamX 3.0. N-terminus and prolines were excluded for estimation of exchangeable amides per  
104 peptide.<sup>(32)</sup> All deuterium exchange experiments were performed in triplicate and reported values  
105 are not corrected for deuterium back exchange.

106

## 107 **Modelling and molecular dynamics (MD) simulations**

108 An integrative model of full-length SARS-CoV-2 S protein was built using Modeller v9.21.(33)  
109 The cryo-EM structure of pre-fusion S ectodomain in the open conformation (PDB: 6VSB)(29)  
110 was used as the template for the ectodomain (ECD) with missing loops on the NTD modelled  
111 based on SARS S NTD crystal structure (PDB: 5X4S).(34) The NMR structure of SARS S HR2  
112 domain (PDB: 2FXP)(35) was used as the template for the HR2 domain, while the TM domain  
113 was modelled using the NMR structure of the HIV-1 gp-41 TM domain (PDB: 5JYN)(36). Ten  
114 models were built and subjected to stereochemical assessment using the discreet optimized protein  
115 energy (DOPE) score(37) and Ramachandran analysis.(38) The model with the lowest DOPE score  
116 and the smallest number of Ramachandran outliers was chosen. Palmitoylation was added to three  
117 cysteine residues (C1236, C1240 and C1243) on the CT domain based on a study showing its  
118 importance in SARS S protein function.(39) The S protein model was then embedded into a model  
119 membrane representing the endoplasmic reticulum-Golgi intermediate compartment  
120 (ERGIC),(40) where coronaviruses are known to assemble in a bud form.(41, 42) The ERGIC  
121 model membrane was built using CHARMM-GUI Membrane Builder.(43) All-atom MD  
122 simulation was performed for 200 ns using GROMACS 2018(44) and the CHARMM36 force  
123 field.(45) The systems were solvated with TIP3P water molecules and 0.15 M NaCl salt.  
124 Minimization and equilibration were performed following standard CHARMM-GUI  
125 protocols.(46) Temperature was maintained at 310 K using the Nosé-Hoover thermostat(47, 48)  
126 and the pressure was maintained at 1 atm using the Parrinello-Rahman barostat.(49) Electrostatics  
127 were calculated using the smooth particle mesh Ewald (PME) method(50) with a real space cut-  
128 off of 1.2 nm and the van der Waals were truncated at 1.2 nm with force switch smoothing between  
129 1.0 to 1.2 nm. Constraints were applied to covalent bonds with hydrogen atoms using the LINCS  
130 algorithm(51) and a 2 fs integration time step was employed. For simulations of the ACE2  
131 receptor, the cryo-EM structure of ACE2-B<sup>0</sup>AT1 complex in the open conformation (PDB:  
132 6M1D)(52) was used. The ACE2-B<sup>0</sup>AT1 complex was embedded into a model membrane  
133 representing the epithelial cell membrane.(53, 54) All-atom MD simulation was performed for 200  
134 ns using the protocols described above. Principal component analysis (PCA) and root means  
135 square fluctuation (RMSF) analyses were performed using GROMACS, and simulations were  
136 visualized in VMD.(55)

137

138

## 139 Supplementary References

- 140 29. D. Wrapp *et al.*, Cryo-EM structure of the 2019-nCoV spike in the prefusion conformation.  
141 *Science* **367**, 1260-1263 (2020).
- 142 30. Y. Hamuro, S. J. Coales, K. S. Molnar, S. J. Tuske, J. A. Morrow, Specificity of immobilized porcine  
143 pepsin in H/D exchange compatible conditions. *Rapid Commun Mass Spectrom* **22**, 1041-1046  
144 (2008).
- 145 31. Y. Watanabe, J. D. Allen, D. Wrapp, J. S. McLellan, M. Crispin, Site-specific glycan analysis of the  
146 SARS-CoV-2 spike. *Science* **369**, 330-333 (2020).
- 147 32. A. N. Hoofnagle, K. A. Resing, N. G. Ahn, Protein analysis by hydrogen exchange mass  
148 spectrometry. *Annu Rev Biophys Biomol Struct* **32**, 1-25 (2003).
- 149 33. A. Sali, T. L. Blundell, Comparative protein modelling by satisfaction of spatial restraints. *J Mol*  
150 *Biol* **234**, 779-815 (1993).
- 151 34. Y. Yuan *et al.*, Cryo-EM structures of MERS-CoV and SARS-CoV spike glycoproteins reveal the  
152 dynamic receptor binding domains. *Nat Commun* **8**, 15092 (2017).
- 153 35. S. Hakansson-McReynolds, S. Jiang, L. Rong, M. Caffrey, Solution structure of the severe acute  
154 respiratory syndrome-coronavirus heptad repeat 2 domain in the prefusion state. *J Biol Chem*  
155 **281**, 11965-11971 (2006).
- 156 36. J. Dev *et al.*, Structural basis for membrane anchoring of HIV-1 envelope spike. *Science* **353**, 172-  
157 175 (2016).
- 158 37. D. Eramian *et al.*, A composite score for predicting errors in protein structure models. *Protein Sci*  
159 **15**, 1653-1666 (2006).
- 160 38. G. N. Ramachandran, C. Ramakrishnan, V. Sasisekharan, Stereochemistry of polypeptide chain  
161 configurations. *J Mol Biol* **7**, 95-99 (1963).
- 162 39. C. M. Petit *et al.*, Palmitoylation of the cysteine-rich endodomain of the SARS-coronavirus spike  
163 glycoprotein is important for spike-mediated cell fusion. *Virology* **360**, 264-274 (2007).
- 164 40. G. van Meer, Lipids of the Golgi membrane. *Trends Cell Biol* **8**, 29-33 (1998).
- 165 41. J. Krijnse-Locker, M. Ericsson, P. J. Rottier, G. Griffiths, Characterization of the budding  
166 compartment of mouse hepatitis virus: evidence that transport from the RER to the Golgi  
167 complex requires only one vesicular transport step. *J Cell Biol* **124**, 55-70 (1994).
- 168 42. J. Klumperman *et al.*, Coronavirus M proteins accumulate in the Golgi complex beyond the site  
169 of virion budding. *J Virol* **68**, 6523-6534 (1994).
- 170 43. J. Lee *et al.*, CHARMM-GUI Membrane Builder for Complex Biological Membrane Simulations  
171 with Glycolipids and Lipoglycans. *J Chem Theory Comput* **15**, 775-786 (2019).
- 172 44. M. J. Abraham *et al.*, GROMACS: High performance molecular simulations through multi-level  
173 parallelism from laptops to supercomputers. *SoftwareX* **1-2**, 19-25 (2015).
- 174 45. J. Huang, A. D. MacKerell, Jr., CHARMM36 all-atom additive protein force field: validation based  
175 on comparison to NMR data. *J Comput Chem* **34**, 2135-2145 (2013).
- 176 46. J. Lee *et al.*, CHARMM-GUI Input Generator for NAMD, GROMACS, AMBER, OpenMM, and  
177 CHARMM/OpenMM Simulations Using the CHARMM36 Additive Force Field. *J Chem Theory*  
178 *Comput* **12**, 405-413 (2016).
- 179 47. S. Nosé, A molecular dynamics method for simulations in the canonical ensemble. *Molecular*  
180 *Physics* **52**, 255 (1984).
- 181 48. W. G. Hoover, Canonical dynamics: Equilibrium phase-space distributions. *Physical Review A* **31**,  
182 1695-1697 (1985).
- 183 49. M. Parrinello, A. Rahman, Polymorphic transitions in single crystals: A new molecular dynamics  
184 method. *Journal of Applied Physics* **52**, 7182-7190 (1981).



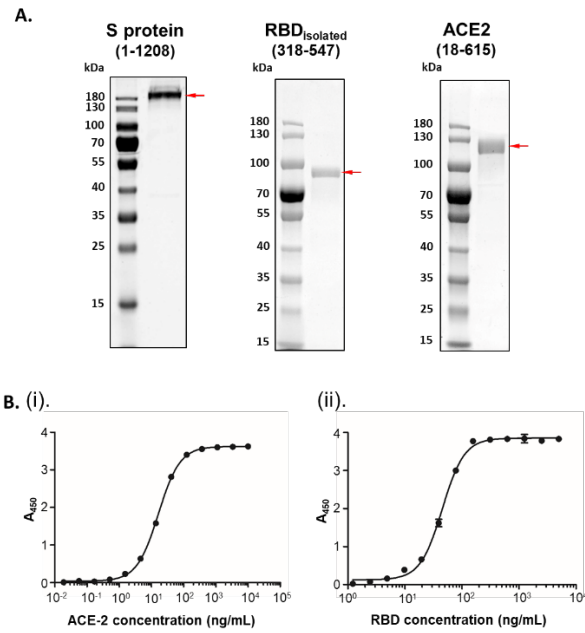
- 185 50. U. Essmann *et al.*, A smooth particle mesh Ewald method. *The Journal of Chemical Physics* **103**,  
186 8577-8593 (1995).
- 187 51. B. Hess, H. Bekker, H. J. C. Berendsen, J. G. E. M. Fraaije, LINCS: A linear constraint solver for  
188 molecular simulations. *Journal of Computational Chemistry* **18**, 1463-1472 (1997).
- 189 52. R. Yan *et al.*, Structural basis for the recognition of SARS-CoV-2 by full-length human ACE2.  
190 *Science* **367**, 1444-1448 (2020).
- 191 53. H. P. Jia *et al.*, ACE2 receptor expression and severe acute respiratory syndrome coronavirus  
192 infection depend on differentiation of human airway epithelia. *J Virol* **79**, 14614-14621 (2005).
- 193 54. J. L. Sampaio *et al.*, Membrane lipidome of an epithelial cell line. *Proc Natl Acad Sci U S A* **108**,  
194 1903-1907 (2011).
- 195 55. W. Humphrey, A. Dalke, K. Schulten, VMD: visual molecular dynamics. *J Mol Graph* **14**, 33-38,  
196 27-38 (1996).

197

198

199 **Supplementary Figures**

200

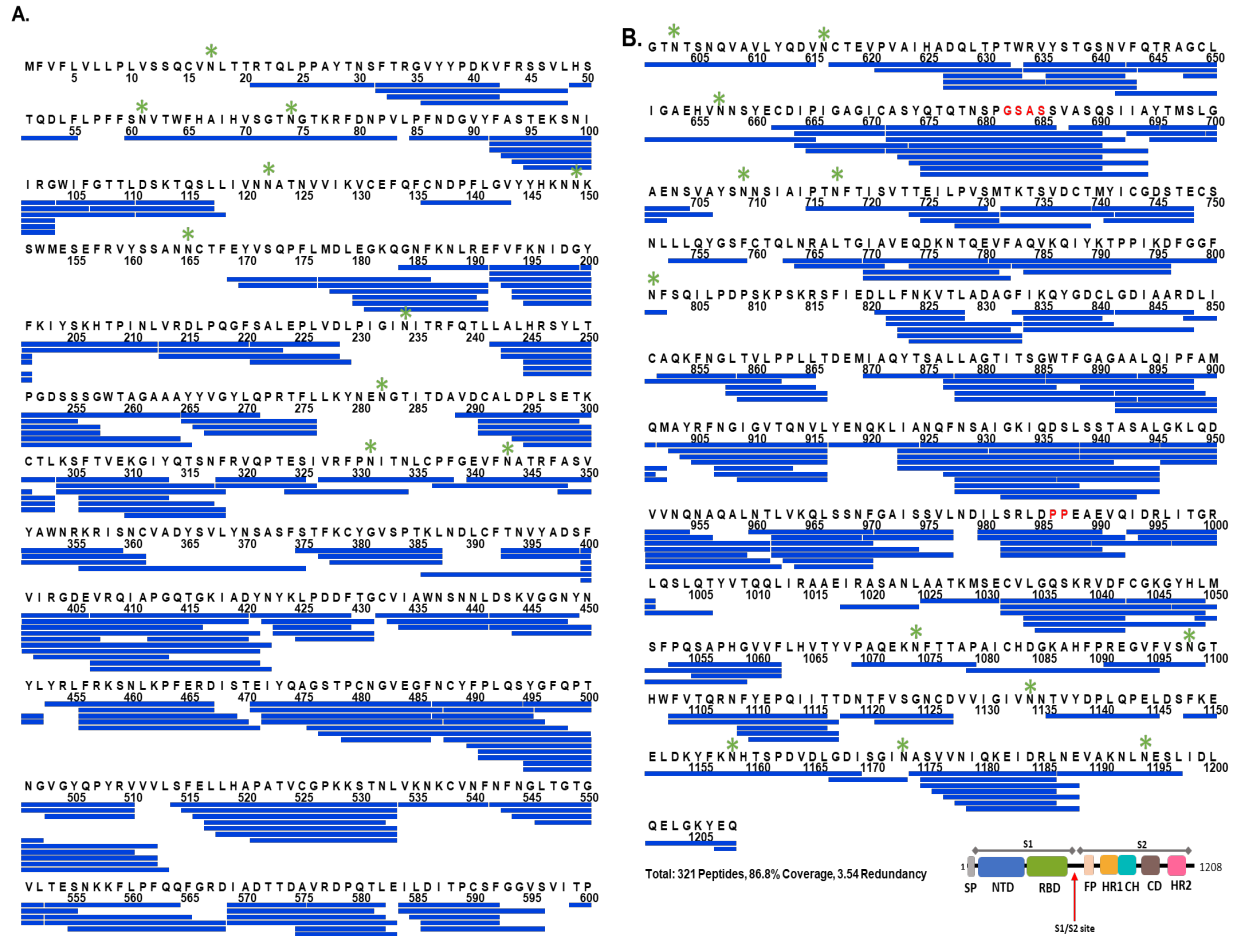


201

202 **Figure S1:**

203 **Homogeneity of protein samples.** (A) Images of denaturing polyacrylamide gel electrophoresis  
204 of purified proteins of the S protein (mutant), isolated RBD and ACE2 are shown, and their  
205 molecular sizes are highlighted with red arrow, alongside protein standards. Domain organization  
206 is shown for reference. (B) Interactions between ACE2 and RBD represented by the binding  
207 curves.





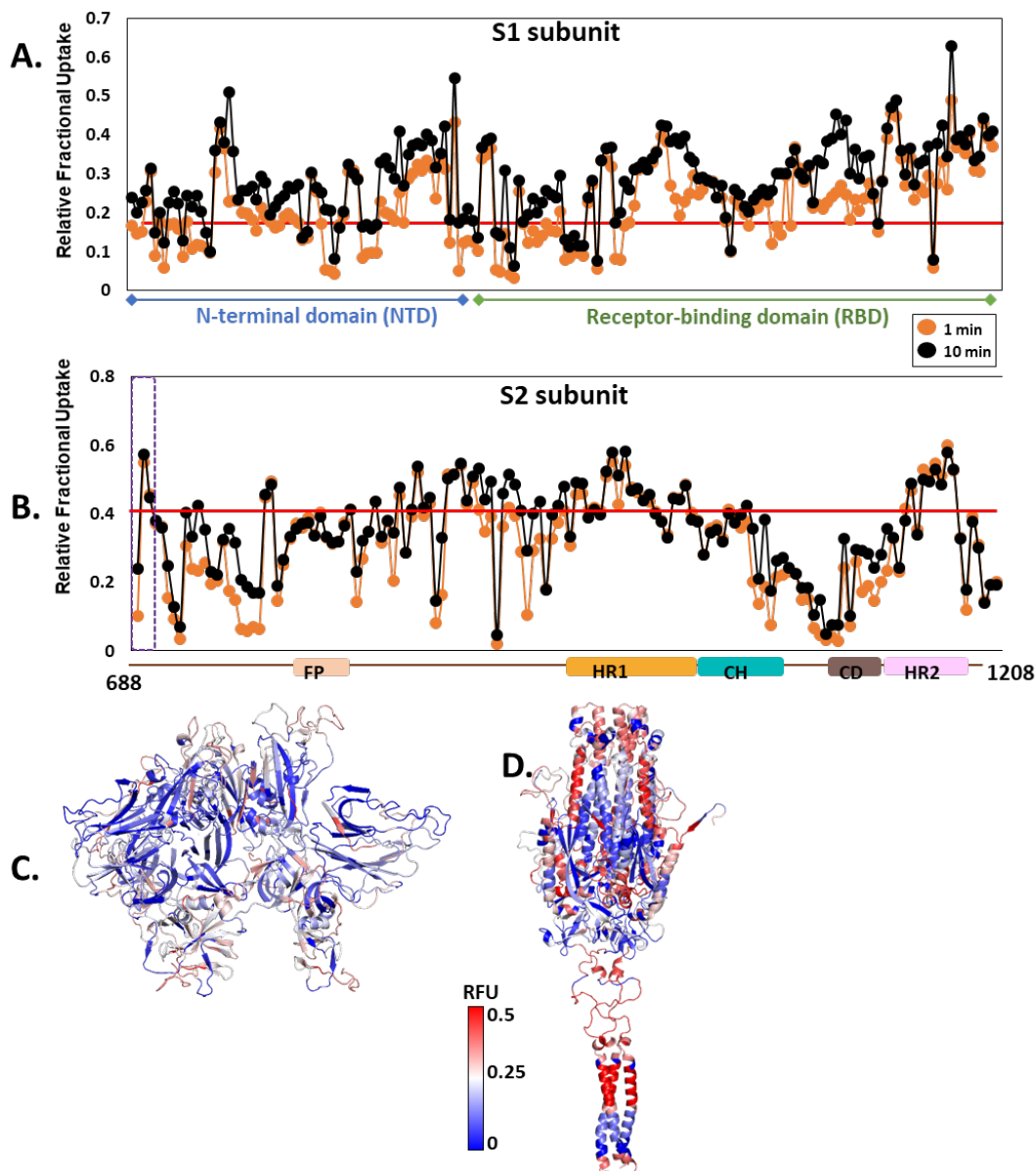
208

209

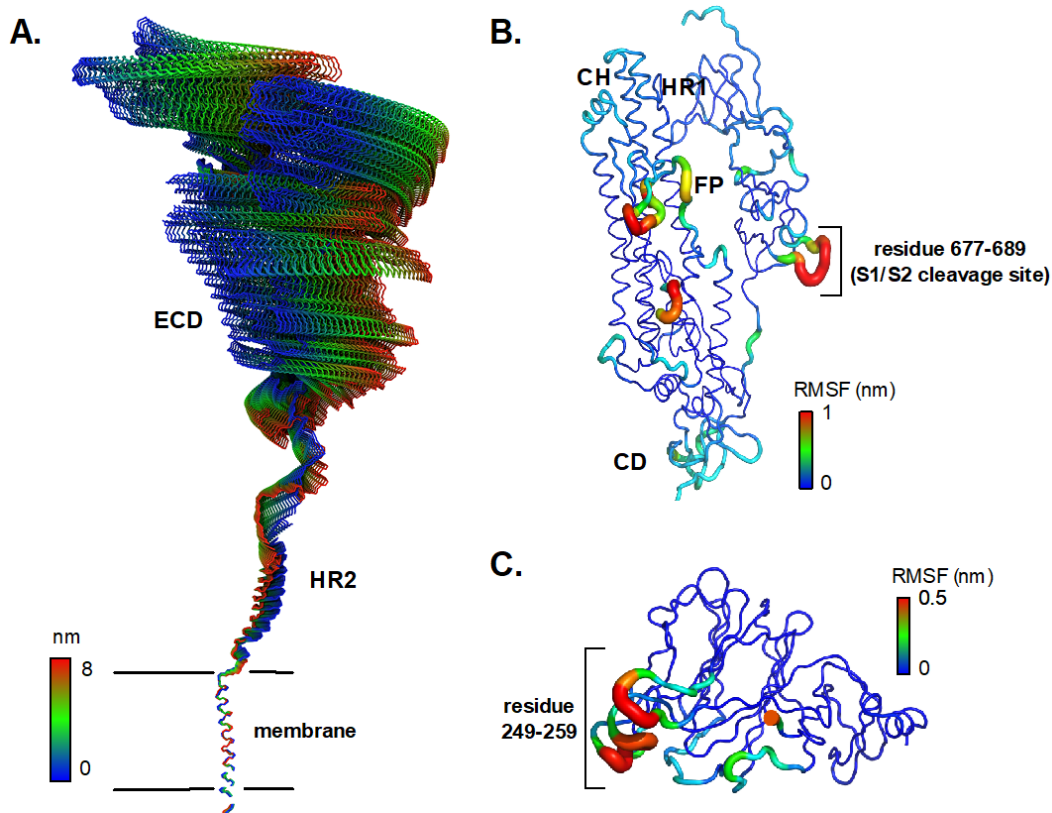
210 **Figure S2:**

211 **Primary sequence coverage map of pepsin proteolysed peptides of the S protein.** Coverage  
212 map showing 321 peptides spanning 87% of the S protein: (A) 1 – 600 and (B) 601 – 1208, with  
213 the mutations highlighted in red. Glycosylation sites are indicated by asterisks (\*) and peptide  
214 coverage for C-terminal twin strep-tag is not shown. The domain organization for S protein  
215 construct 1-1208 is shown.

216



217  
218 **Figure S3:**  
219 **Time dependent changes in deuterium exchange for free S protein.** Deuterium uptake of each  
220 pepsin proteolysed peptide listed from N-to C-terminus (X-axis) spanning S1 subunit (A) and  
221 S2 subunit (B) at deuterium labelling times 1 min and 10 min are represented as relative fractional  
222 uptake (RFU, Y-axis) values. Red line indicates the average RFU value. RFU values at 1 min of  
223 deuterium labelling time mapped on to the structures of the S1 (C) and S2 (D) subunits. High and  
224 low exchanging regions are as per key.  
225

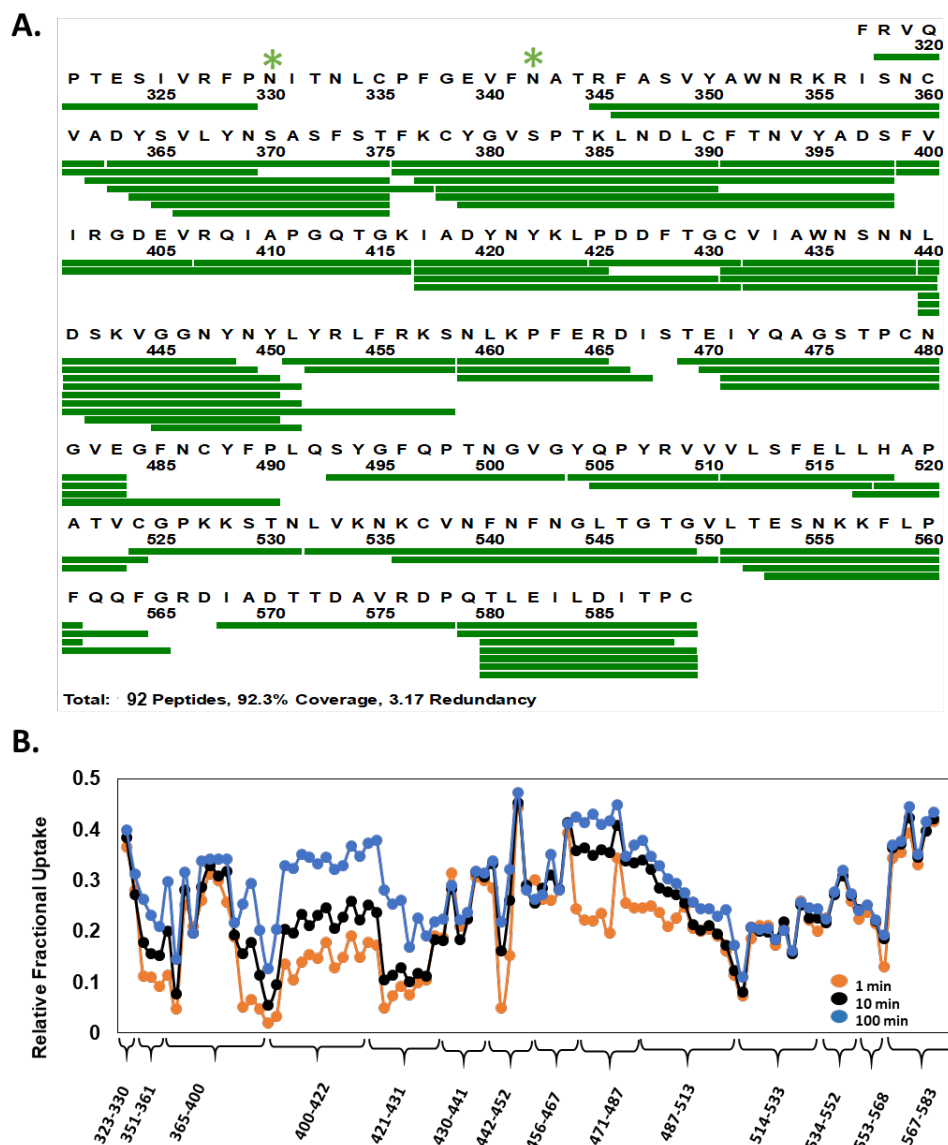


226

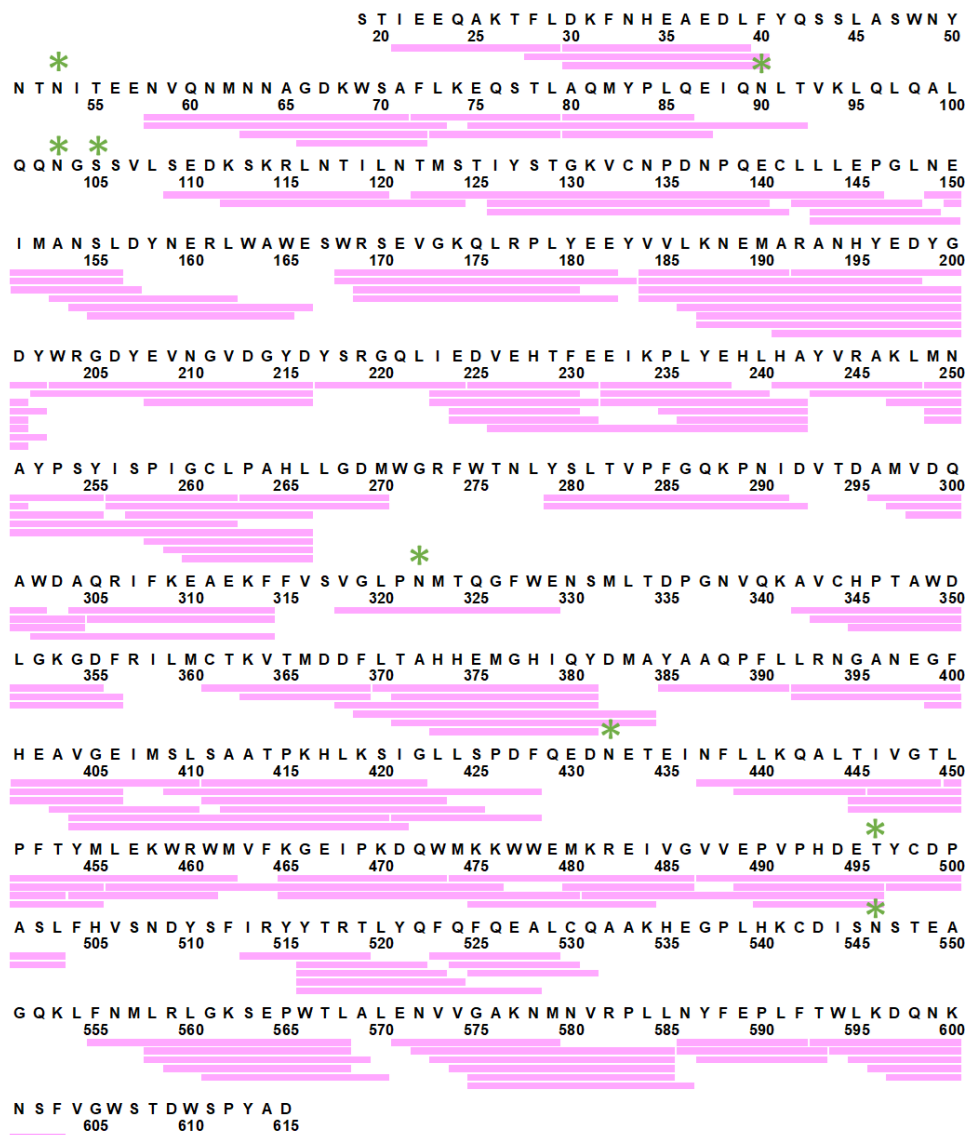
227

**Figure S4:**

228 **Dynamics of the S protein trimer from all-atom MD simulation.** (A) The first principal motion  
229 of all backbone atoms for the full-length S protein during all-atom MD simulations as determined  
230 by principal component analysis (PCA). (B-C) RMSF values of backbone atoms on the S2 subunits  
231 and NTD. Residues with high RMSF are labelled.



232  
 233 **Figure S5:**  
 234 **Primary sequence coverage and deuterium exchange profile of RBD<sub>isolated</sub>.** (A) Coverage map  
 235 showing 92 peptides (green bar) spanning ~92% sequence of MBP-RBD<sub>isolated</sub> (318-589) fusion  
 236 protein. N-terminal maltose-binding protein (MBP) affinity-tag is not shown. Glycosylation sites  
 237 are indicated by green asterisk. (B) RFU plot of pepsin proteolyzed peptides of RBD<sub>isolated</sub> listed  
 238 N-to C-terminus for deuterium labelling times as per key.



Total: 146 Peptides, 80.2% Coverage, 3.35 Redundancy

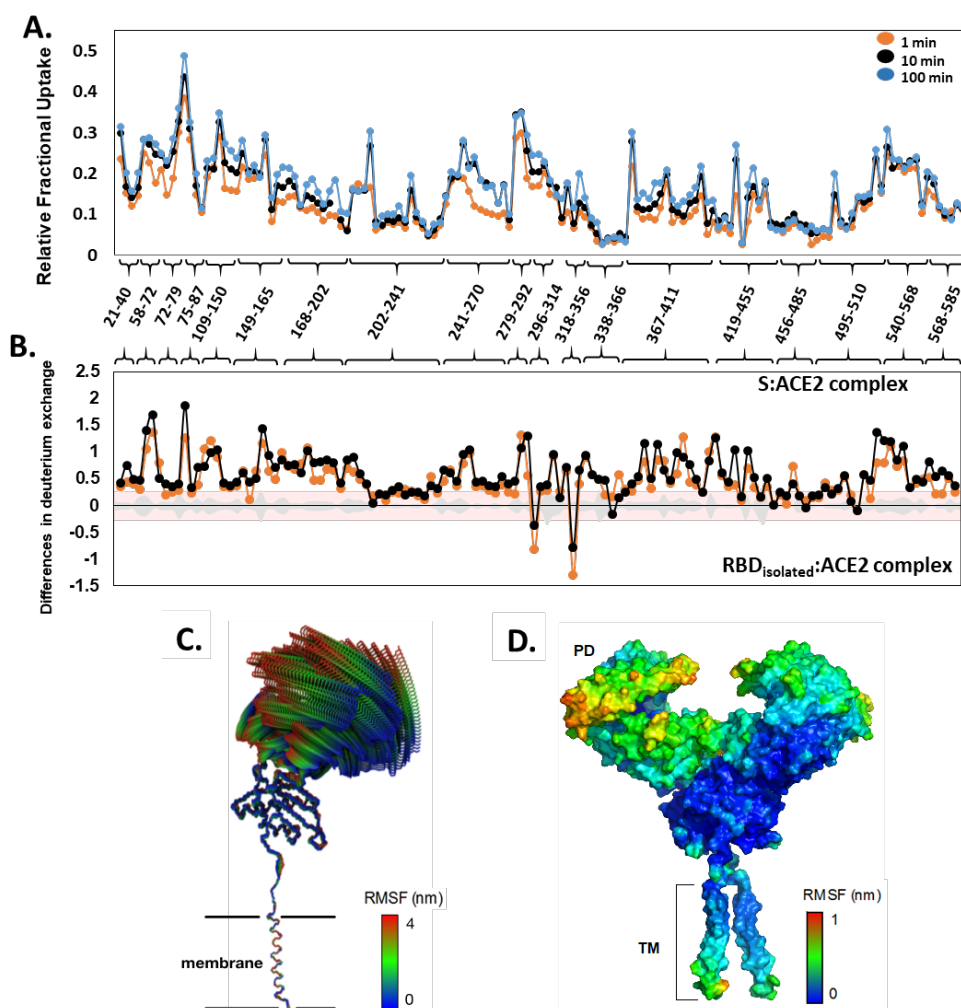
239

240

241 **Figure S6: Pepsin digest map and sequence coverage ACE2.**

242 (A) Coverage map showing 140 peptides (pink horizontal bars) covering ~80% sequence of ACE2

243 (18-615). Sequence of FC-tag is not shown. Glycosylation sites are represented by green asterisk.



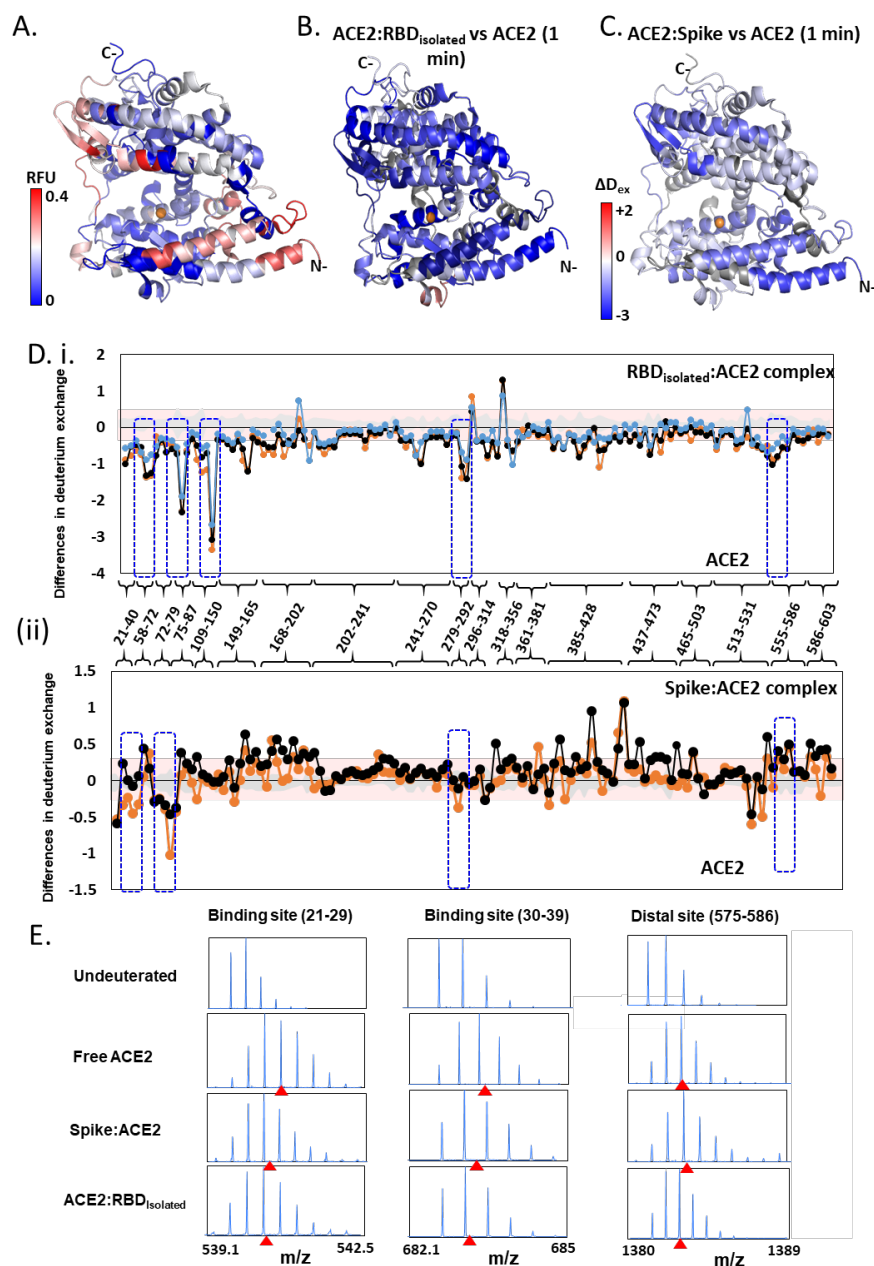
244

245

246 **Figure S7: Deuterium uptake profile for ACE2 receptor and all-atom MD simulation of the**  
247 **ACE2-B0AT1 complex.**

248 (A) RFU values of pepsin proteolysed peptides listed in N-to C-terminus of ACE2 (peptide 18-  
249 615) for deuterium labelling times are shown. (B) Differences in deuterium exchange (Y-axis) of  
250 ACE2 peptides listed from N-to C-terminus (X-axis) between S:ACE2 complex and  
251 RBD<sub>isolated</sub>:ACE2 complex. Deuterium exchange significance threshold of  $\pm 0.3$  D is indicated  
252 in red and standard errors in gray. (C) The first principal motion of the all backbone atoms of the  
253 ACE2 monomer as determined by PCA. (D) The RMSF values of the ACE2 receptor mapped onto  
254 the surface of the ACE2.

255



256  
257

258 **Figure S8: Effect of RBD<sub>isolated</sub> and RBDs complexes on ACE2 dynamics.**  
 259 (A) Structure of extracellular domain of ACE2 receptor (PDB ID: 1R42) depicting the RFU at  $t$   
 260  $= 1$  min. (B) Differences in deuterium exchange of RBD<sub>isolated</sub>:ACE2 complex and free ACE2 at  $t$   
 261  $= 1$  min is mapped onto the structure of ACE2, predominantly showing decreased deuterium  
 262 exchange in ACE2 (shades of blue). (C) Heat map of differences in deuterium exchange ( $t = 1$   
 263 min) of S:ACE2 complex and free ACE2. (D) Plot showing differences in deuterium exchange  
 264 between ACE2 and complexes with RBD (i) and S (ii) at different labeling times. Pepsin digest  
 265 fragments are indicated by their residue numbers. Cutoff  $\pm 0.3$  D is the deuterium exchange  
 266 significance threshold, indicated by pink shaded box, and standard errors are in gray. Positive



267 differences denote increased deuterium exchange in (i) RBD:ACE2 or (ii) S:ACE2 compared to  
268 free ACE2, while negative differences denote decreased deuterium exchange. Peptides spanning  
269 the sites of interaction with RBD and two distal sites (278-292, 574-585) are highlighted. (E)  
270 Stacked mass spectra showing isotopic distribution for select peptides spanning the binding sites  
271 (21-29, 30-39) and a distal allosteric site (575-586) for ACE2, S:ACE2 and RBDisolated:ACE2  
272 are shown at 1 min deuterium labeling time. Centroids indicated by red arrow-heads.  
273

#### 274 **Data S1 to S3**

##### 275 **Table S1:**

276 Relative Fraction uptake values at various deuterium labeling times for Spike and S:ACE2  
277 complex  
278

##### 279 **Table S2:**

280 Relative Fractional Uptake values at various deuterium labeling times for free and ACE2-bound  
281 RBD (isolated)  
282

##### 283 **Table S3:**

284 Relative Fractional Uptake values at various deuterium labeling times for free ACE2 and its  
285 complexes with isolated RBD and Spike protein  
286